

TD-BFR: Truncated Diffusion Model for Efficient Blind Face Restoration

Ziying Zhang¹ Xiang Gao¹ Zhixin Wang¹ Qiang Hu^{1†} Xiaoyun Zhang^{1†}

¹Cooperative Medianet Innovation Center, Shanghai Jiao Tong University, Shanghai, China

{zyzhang2000, frxg0918, dedsec_z, qiang.hu, xiaoyun.zhang}@sjtu.edu.cn

Abstract—Diffusion-based methodologies have shown significant potential in blind face restoration (BFR), leveraging their robust generative capabilities. However, they are often criticized for two significant problems: 1) slow training and inference speed, and 2) inadequate recovery of fine-grained facial details. To address these problems, we propose a novel Truncated Diffusion model for efficient Blind Face Restoration (TD-BFR), a three-stage paradigm tailored for the progressive resolution of degraded images. Specifically, TD-BFR utilizes an innovative truncated sampling method, starting from low-quality (LQ) images at low resolution to enhance sampling speed, and then introduces an adaptive degradation removal module to handle unknown degradations and connect the generation processes across different resolutions. Additionally, we further adapt the priors of pre-trained diffusion models to recover rich facial details. Our method efficiently restores high-quality images in a coarse-to-fine manner and experimental results demonstrate that TD-BFR is, on average, $4.75\times$ faster than current state-of-the-art diffusion-based BFR methods while maintaining competitive quality.

Index Terms—Blind face restoration, Diffusion model, Efficient

I. INTRODUCTION

Image restoration aims to reconstruct a high-quality image from its LQ observation. In typical image restoration problems such as denoising, deblurring, and super-resolution, the degradation process is simple and known (e.g., bicubic downsampling), while blind face restoration (BFR) endeavors to recover high-quality facial images from their degraded counterparts, which may involve various forms of degradation.

Recent research efforts like CodeFormer [1], GFPGAN [2] integrate potent generative facial priors, to produce faithful and high-quality facial details. In recent years, denoising diffusion probabilistic models [3] have demonstrated remarkable performance in image generation. Building upon this, various approaches, such as DR2 [4] and StableSR [5], have integrated DDPMs as an additional prior, enhancing their generative capabilities beyond traditional GAN-based methods. However, these methods prioritize image quality, sacrificing time efficiency by relying on complete diffusion model processes. Specifically, while StableSR and DifFace [6] have demonstrated promising results with the help of powerful priors of diffusion models, it demands more than 50 sampling steps for restoring a single LQ face image, resulting in significant time expenditure. To improve sampling efficiency in diffusion models, TDPM [7] and RDM [8] propose to synthesize the image by merely using the partial generation process, which, in a faster manner, adds noise not until the data becomes pure random noise and use fewer reverse steps to generate

data. Meanwhile, for the BFR task, EDBFR [9] addresses the lengthy sampling steps of diffusion-based methods by designing additional network modules to accelerate. However, the restored images often suffer from blurriness lacking details. Consequently, there is a critical demand for developing more efficient methodologies capable of ensuring high-quality face restoration images without compromising sampling efficiency.

In this paper, we propose the Truncated Diffusion model for BFR (TD-BFR), which adopts a three-stage paradigm designed to enhance the efficiency of diffusion-based methods while preserving the restoration quality. Inspired by [8], we find that the intermediate variables of diffusion models at different resolutions exhibit similar noise distributions across specific steps (shown in (a) and (b), distinct from (c) of Fig. 1), mitigating the effects of degradation and resolution discrepancies. Therefore, our method decomposes the BFR task into a series of multi-stage processing steps to explicitly reduce the time burden of the restoration process by progressively addressing different resolutions of the input images. Initially, we employ a *Low-resolution Startup (LRS)* to integrate low-quality images into the diffusion model by exchanging their low-frequency components with those of the intermediate variable using a low-pass filter at low resolution. Next, the *Adaptive Degradation Remover (ADR)* dynamically selects the cutoff frequency to produce a smooth face image with reduced fine-grained details. Finally, we use *Generative Detail Boost (GDB)*, which fine-tunes pre-trained text-to-image diffusion models [10] to generate accurate and visually pleasing image details. Quantitative experiments demonstrate that TD-BFR significantly improves sampling efficiency, achieving a restoration speed of **3.53s** per image while other state-of-the-art diffusion based methods need 8.76s \sim 25.05s (Tab. I). The main contributions of our paper are as follows:

- We propose TD-BFR, a method that leverages the partial generation process to decompose the BFR task into three progressive multi-scale stages, significantly enhancing the sampling speed.
- We propose ADR, a module that dynamically addresses unknown degradation while serving as a bridge between the low-resolution integration in the first stage and the detail enhancement in the third stage, ensuring high-quality face restoration.
- Comprehensive experiments demonstrate the superiority of methods in both competitive quality and efficiency with sampling speed enhancement of **4.75** \times on average.

[†] Corresponding author.

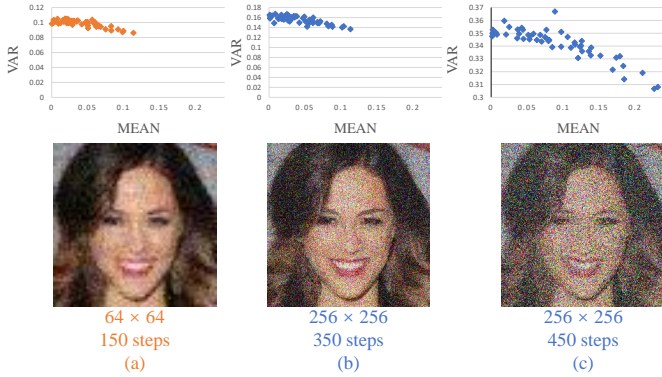


Figure 1. (a) presents the mean and variance of $(q(x_t|x_0) - q(x_0))$, and the visualized result at 150 steps for the 64-resolution diffusion model. (b) and (c) shows the corresponding data at 350 and 450 steps for the 256 resolution.

II. METHODOLOGY

A. Preliminary

Denoising Diffusion Probabilistic Models (DDPM) [3] are a class of generative models that first pre-defines a variance schedule $\{\beta_1, \beta_2, \dots, \beta_T\}$ to progressively corrupt an image x_0 to a noisy status through forward (diffusion) process:

$$q(x_t|x_{t-1}) = \mathcal{N}(x_t; \sqrt{1 - \beta_t}x_{t-1}, \beta_t\mathbf{I}), \quad (1)$$

Moreover, based on the property of the Markov chain, for any intermediate timestep $t \in \{1, 2, \dots, T\}$, the corresponding noisy distribution has an analytic form:

$$\begin{aligned} q(x_t|x_0) &= \mathcal{N}(x_t; \sqrt{\bar{\alpha}_t}x_0, (1 - \bar{\alpha}_t)\mathbf{I}) \\ &= \sqrt{\bar{\alpha}_t}x_0 + \sqrt{1 - \bar{\alpha}_t}\epsilon, \end{aligned} \quad (2)$$

where $\bar{\alpha}_t := \prod_{s=1}^t (1 - \beta_s)$ and $\epsilon \sim \mathcal{N}(\mathbf{0}, \mathbf{I})$. Then $x_T \sim \mathcal{N}(\mathbf{0}, \mathbf{I})$ if T is big enough, usually $T = 1000$.

The model progressively generates images by reversing the forward process. The generative process is also a Gaussian transition with the learned mean μ_θ :

$$p_\theta(x_{t-1}|x_t) = \mathcal{N}(x_{t-1}; \mu_\theta(x_t, t), \sigma_t^2\mathbf{I}), \quad (3)$$

where σ_t is usually a pre-defined constant related to the variance schedule, and $\mu_\theta(x_t, t)$, is usually parameterized by a denoising U-Net $\epsilon_\theta(x_t, t)$ [3] with the following equivalence:

$$\mu_\theta(x_t, t) = \frac{1}{\sqrt{\alpha_t}}(x_t - \frac{1 - \alpha_t}{\sqrt{1 - \bar{\alpha}_t}}\epsilon_\theta(x_t, t)). \quad (4)$$

B. Framework Overview

In Fig. 1, we examine the noise level similarity of intermediate variables across resolutions and steps. The mean and variance of $(q(x_t|x_0) - q(x_0))$ are calculated to evaluate noise consistency, as shown in the first row of Fig. 1. The VAR-MEAN figures indicate that the noise level of the 150-step variable at 64 resolution aligns closely with the 350-step variable at 256 resolution but differs from the 450-step. These findings, consistent with the visual results in the second row of Fig. 1, demonstrate that smooth truncation-stitching can be achieved by adjusting breakpoints, enabling a progressive multi-stage, multi-resolution framework.

To better optimize breakpoint selection and model truncation across different resolutions, inspired by [8], we analyze

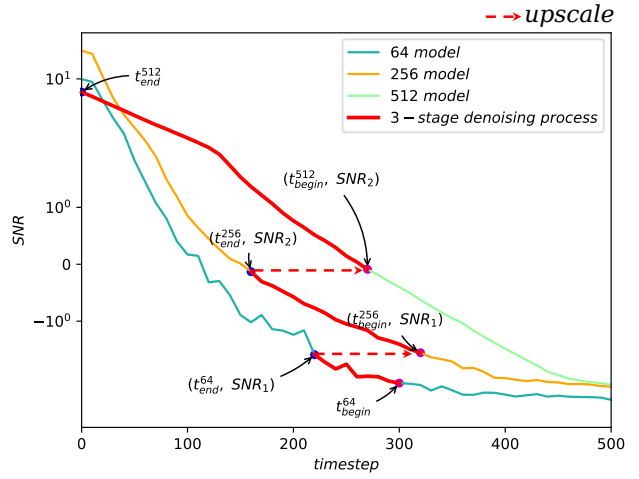


Figure 2. The Signal-to-noise ratio (SNR) curves of diffusion models at different resolutions. The breakpoints for truncated diffusion models can be selected based on similar SNR values, such as $SNR(t_{end}^{64}) \approx SNR(t_{begin}^{256})$.

the signal-to-noise ratio (SNR) curves of diffusion models at various resolutions, as shown in Fig. 2. The SNR quantifies the proportion of image semantics at the pixel level, and is defined by:

$$SNR(t) := 10 \lg \frac{\sum_{i=0}^{M-1} \sum_{j=0}^{N-1} x_t(i, j)^2}{\sum_{i=0}^{M-1} \sum_{j=0}^{N-1} [x_t(i, j) - x_0(i, j)]^2}. \quad (5)$$

Since SNR varies with resolution for the same number of steps, selecting appropriate breakpoints is essential for partial generative processes. To ensure consistent semantic proportions, breakpoints are determined based on comparable SNR values. For instance, transitioning from 64 to 256 resolution uses the SNR_1 value at the 64-resolution breakpoint as the starting point for the 256-resolution model, guiding step selection according to the lower-resolution SNR.

Building on this, our proposed truncated framework, TD-BFR, shown in Fig. 3, adopts a three-stage paradigm to restore degraded images of varying resolutions progressively. The first stage, Low-Resolution Startup (LRS), integrates the LQ image into the diffusion model at a low resolution. The second stage, Adaptive Degradation Remover (ADR), addresses unknown degradations and transitions between resolutions. Finally, the third stage, Generative Detail Boost (GDB), leverages the fine-tuned diffusion model's priors to generate detailed, high-quality facial features, significantly enhancing restoration quality and sampling efficiency.

C. Truncated Diffusion model for efficient BFR

Stage One: Low-resolution Startup(LRS). Due to the substantial computational demands of high-resolution diffusion models, we advocate for implementing an LRS, such as a 64-resolution initialization, utilizing the input LQ y . Proved by [4], (1) there exists an intermediate timestep t_{end} such that for $t > t_{end}$, the distance between $q(x_t|x)$ and $q(y_t|y)$ is close especially in the low-frequency part; (2) there exists $t_{begin} > t_{end}$ such that the distance between $(x_{t_{end}}$ is abbreviated as x_{end}) $q(x_{begin}|x)$ and $q(y_{begin}|y)$ is eventually small enough, satisfying $q(x_{begin}|x) \approx q(y_{begin}|y)$.

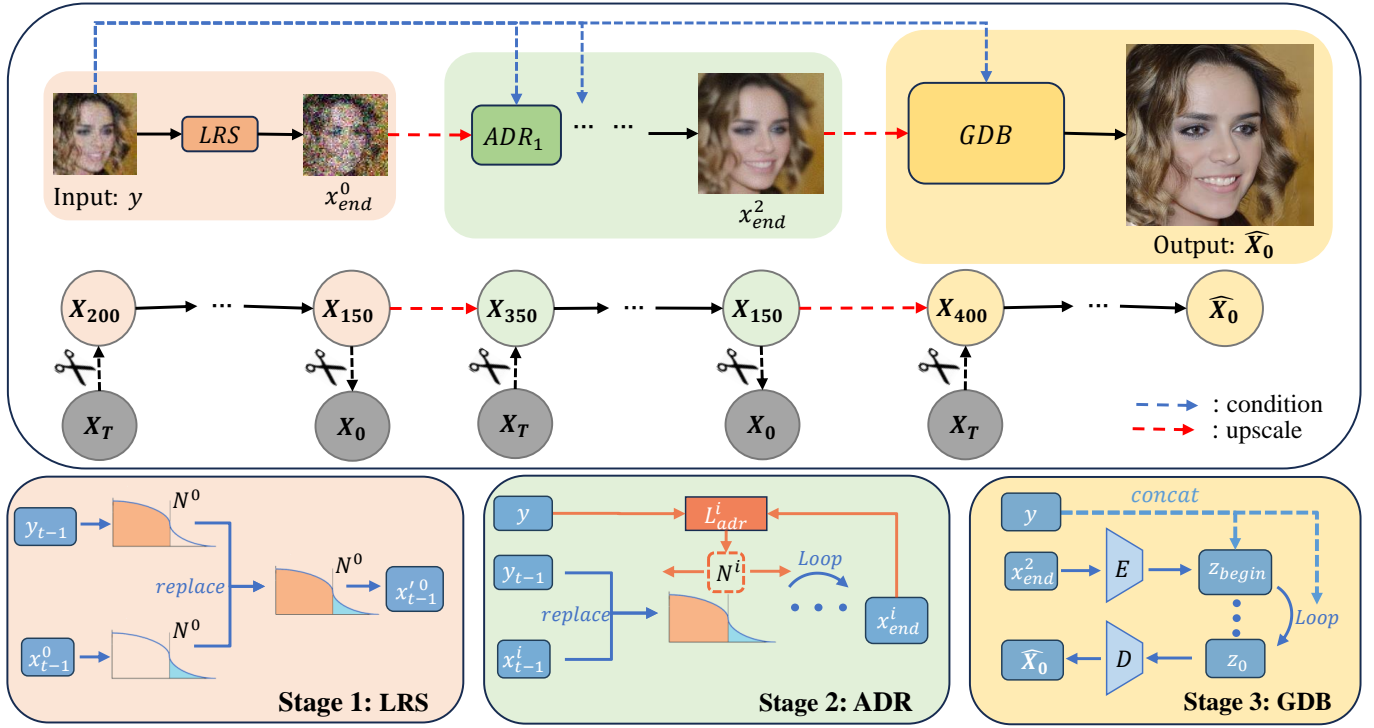


Figure 3. Overall TD-BFR: A three-stage paradigm tailoring for progressive resolution of the input image. ADR serves as a bridge for adaptive handling of unknown degradation and resolution variance, enabling low-resolution integration via LRS and detail generation via GDB.

Hence, the initial stage involves employing a truncated diffusion process at lower resolutions, utilizing incomplete steps $\{t_{end}^0, \dots, t_{begin}^0\}$, thereby incorporating the LQ images into the entirety of the progressive multi-stage framework.

Let $\Phi_{N^0}(\cdot)$ denote a linear low-pass filtering operation, a sequence of downsampling and upsampling by an initial factor of N^0 , therefore maintaining the dimensionality of the image. After each transition from x_t to x_{t-1} , we sample y_{t-1} from y through Eq. (2). Leveraging the linear property of Φ_{N^0} , we substitute the low-frequency component of x_{t-1} with that of y_{t-1} due to their proximity in distribution [4]. This substitution can be expressed as:

$$x_{t-1}'^0 := \Phi_{N^0}(y_{t-1}) + (\mathbf{I} - \Phi_{N^0})(x_{t-1}^0). \quad (6)$$

In the stage 1 of Fig. 3, the LRS module excludes the high-frequency component of y due to its limited information from degradation. The use of a truncated low-resolution diffusion model introduces minimal time overhead. For BFR with unknown degradation, adding Gaussian noise multiple times to x_t effectively conceals the degradation [4], while low-frequency information retains semantic relevance via linear low-pass filtering $\Phi_{N^0}(\cdot)$. Truncating the forward-reverse diffusion process at low resolution in this stage seamlessly integrates the LQ image into the progressive resolution framework.

Stage Two: Adaptive Degradation Remover(ADR). Based on the severity of degradation caused by the upscaled resolution and the original LQ, ADR is proposed relying on the outcomes x_{end}^0 obtained from LRS. This module automatically adjusts the parameter N^i of the i -th low-pass filter, thereby facilitating BFR and acting as a bridge for resolution transitions. The ADR module can be utilized multiple times

at mid-stage to enhance degradation removal. In this study, we demonstrate its application twice at a resolution of 256 as an illustrative example. For the i -th ADR and the partial time steps $t \in \{t_{end}^i, \dots, t_{begin}^i\}$ based on the SNR curve in Fig. 2, we combine the low-frequency of x with the high-frequency of y to obtain the optimized intermediate variable:

$$x_{t-1}'^i := \Phi_{N^i}(y_{t-1}) + (\mathbf{I} - \Phi_{N^i})(x_{t-1}^i), \quad (7)$$

where x_{t-1}^i denotes the original intermediate variable of the i -th mid-resolution diffusion model. Given the typically unknown severity of degradation in LQ for BFR, previous methods often necessitated manual selection of filter parameters N to extract low-frequency information [4], [11]. To streamline this process while maintaining effective degradation removal, we introduce an ADR, which computes the Mean Squared Error (MSE) loss L_{adr}^i between the restored result x_{end}^i and the input y at the final step, optimizing the parameter N accordingly. The expression for L_{adr}^i is formulated as follows:

$$L_{adr}^i := \frac{1}{mn} \sum_{j=1}^m \sum_{k=1}^n \|\Phi_{N^i}(y)(j, k) - \Phi_{N^i}(x_{end}^i)(j, k)\|^2. \quad (8)$$

When L_{adr}^i exceeds the threshold, which will be discussed in the appendix, the ADR adaptively selects the parameter N^i that matches the severity of the input image y until L_{adr}^i falls below the threshold, to ensure that the semantics of x_{end}^i remain consistent with y during degradation removal and to prevent the restoration result from gradually deviating from the input image y . Additionally, through this operation,

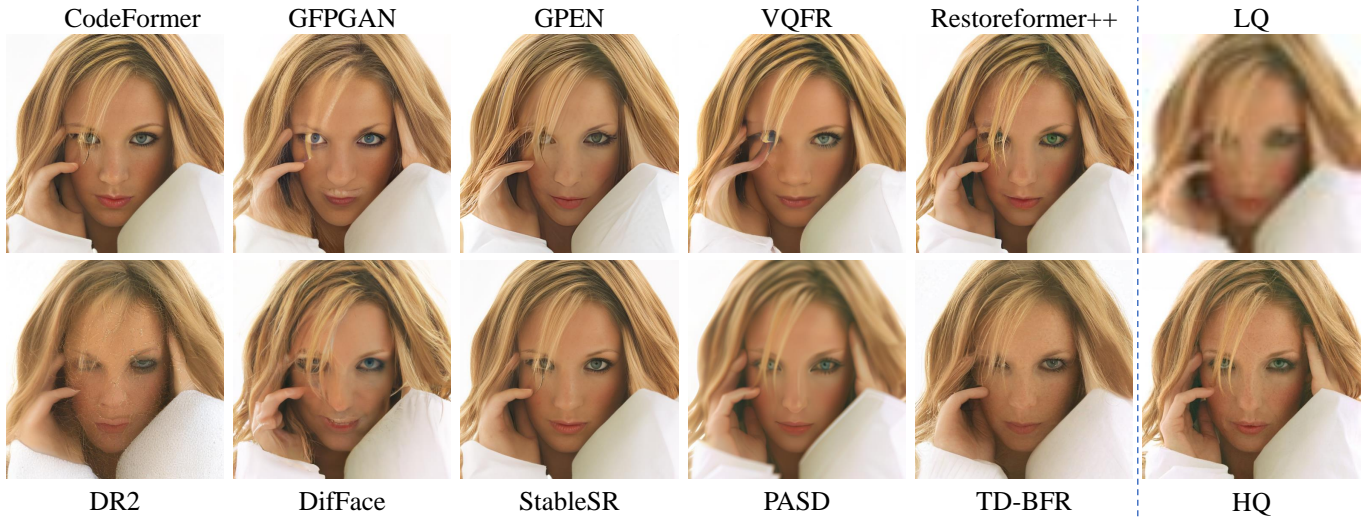


Figure 4. Qualitative comparisons on synthetic CelebA datasets. Our method (TD-BFR) achieves higher restoration quality, encompassing more precise facial details with fewer semantic alterations. (Zoom in for the best view)

the resolution impact caused by multi-scale effects is also mitigated.

Stage Three: Generative Detail Boost(GDB). After the ADR, which retains fundamental semantics but loses high-frequency details, we introduce GDB to enhance image details. GDB leverages the strong priors of large-scale text-to-image diffusion models, such as the Stable Diffusion Model (SDM) [10], to restore realistic details.

In pursuit of refined facial priors, inspired by [12], we fine-tune the SDM by concatenating synthetic degraded images x_{deg} with the noisy latent variable z_t at time t and inputting this into the denoising U-Net $\epsilon_\theta(z_t, t)$. Our optimization objective is to minimize the latent diffusion loss:

$$L = E_{\epsilon(x), x_{deg}, \epsilon \sim \mathcal{N}(\mathbf{0}, \mathbf{I}), t} [\|\epsilon - \epsilon_\theta(\text{cat}(z_t, x_{deg}), t)\|_2^2], \quad (9)$$

Considering the SNR characteristics of diffusion models, we use the fine-tuned truncated SDM in the third stage of our sampling process. The intermediate output x_{end}^2 from the second stage is encoded by $\epsilon(\cdot)$ into latent space, then forwarded to produce the truncated latent result z_{begin} , initiating GDB. Breakpoints for ADR and GDB are chosen based on the SNR properties of the respective resolution. In stage 3 of Fig. 3, we illustrate the truncated sampling process post-SDM fine-tuning. By utilizing SNR properties and the priors of the pre-trained SDM, we perform incomplete denoising to maintain restoration quality comparable to other diffusion methods, while significantly reducing time consumption.

III. EXPERIMENTS

A. Implementation, Datasets, Metrics

Implementation. The complete diffusion models at 64 and 256 resolution employed by stages 1 & 2 are trained on the FFHQ dataset [14]. Following this, we utilize Stable Diffusion

2.1-base [10] as the generative prior. More details on the training will be introduced in the supplementary material.

Test Datasets. We construct one synthetic dataset on CelebA-HQ [15] and three real-world datasets, including WIDER-Test [16], CelebChild, and LFW-Test [17] for testing. The specific explanation for datasets is detailed in the supplementary.

Metrics. For evaluation, we adopt two pixel-wise metrics (PSNR and SSIM), a reference perceptual metric (LPIPS), and two non-reference metrics (NIQE and FID). All metrics are used for the synthetic data while only NIQE and FID are used for real-world datasets due to the lack of HQ images.

B. Efficiency comparison with diffusion-based methods

Since TD-BFR aims to enhance the efficiency of diffusion-based BFR methods, we compare it exclusively with diffusion-based methods. We compare it with DR2 [4] (using SparNetHD [18] as its enhancement module), DifFace [6], StableSR [5], and PASD [13], using their official codes and results. Efficiency is assessed via parameters and inference time, while quality is evaluated using PSNR, LPIPS, NIQE, and FID. As shown in Tab. I, TD-BFR outperforms in quality metrics and achieves an average speed improvement of $4.75\times$. Despite having more parameters, the truncated structure significantly reduces sampling steps, greatly enhancing efficiency.

C. Comparisons with State-of-the-Art Methods

In our comparisons, we contrast TD-BFR with both diffusion-based methods in Efficiency Comparison, and non-diffusion-based methods, including Codeformer [1], GFPGAN [2], GPEN [19], Restoreformer++ [20], VQFR [21], as well as methods based on diffusion models mentioned in Efficiency Comparison.

Synthetic CelebA-Test. Tab. II presents quantitative comparisons on the synthetic CelebA-Test dataset. Our method excels in full-reference metrics (PSNR, LPIPS) and non-reference

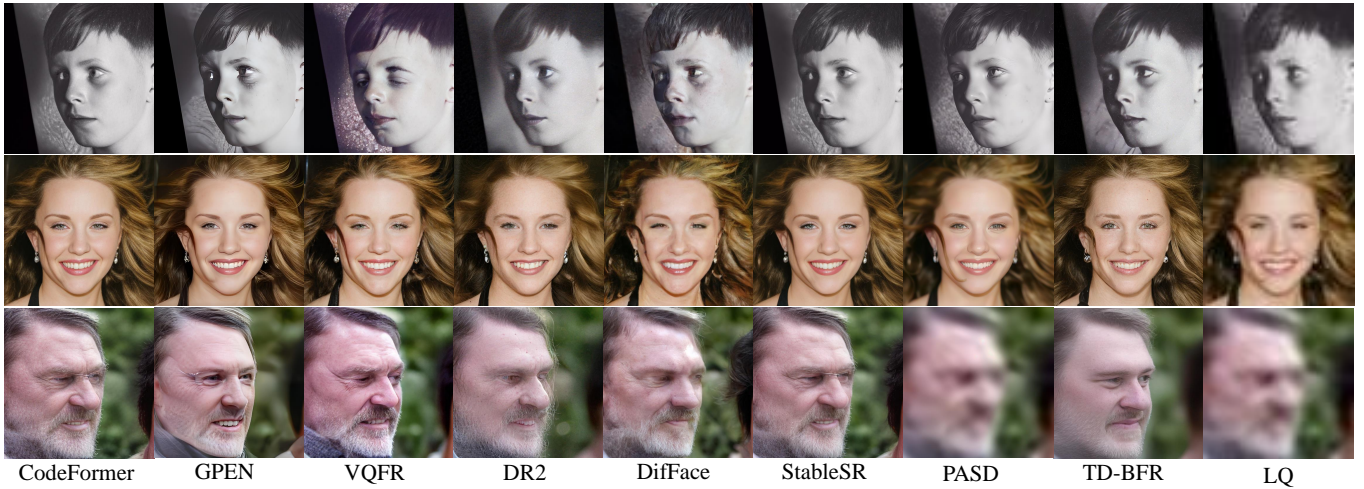


Figure 5. Qualitative comparison with SOTA BFR methods on Celeb-Child (first row), LFW-Test (second row), and WIDER-Test (third row).

Table I

EFFICIENCY COMPARISON ON CELEBA-TEST DATASET. THE SAMPLING TIME RATIO (STR) COMPARES THE TIME CONSUMPTION OF OTHER METHODS WITH OURS, AND SHOWS THAT OTHER METHODS ARE, ON AVERAGE, **4.75** \times SLOWER THAN TD-BFR. **BOLD** AND UNDERLINED INDICATE THE BEST AND THE SECOND BEST PERFORMANCE.

Methods	Params. (M)	PSNR \uparrow	LPIPS \downarrow	NIQE \downarrow	FID \downarrow	Time (s)	STR
DR2 [4]	93.56	23.55	0.434	4.20	50.13	8.76	2.48 \times
DifFace [6]	<u>175.38</u>	25.18	0.461	<u>4.01</u>	<u>48.98</u>	25.04	7.09 \times
StableSR [5]	971.23	24.99	<u>0.361</u>	4.60	50.50	18.33	5.19 \times
PASD [13]	1360.99	<u>25.19</u>	0.419	7.77	67.05	14.90	4.22 \times
TD-BFR(Ours)	1229.48	25.21	0.347	3.99	43.92	3.53	1 \times

Table II

QUANTITATIVE COMPARISONS ON CELEBA-TEST DATASET. **BOLD** AND UNDERLINED INDICATE THE BEST AND THE SECOND BEST PERFORMANCE.

Methods	PSNR \uparrow	SSIM \uparrow	LPIPS \downarrow	NIQE \downarrow	FID \downarrow
CodeFormer	24.81	0.659	<u>0.349</u>	4.52	51.18
GFP-GAN	24.44	0.664	0.377	4.28	48.19
GPEN	24.26	0.665	0.371	5.33	49.66
VQFR	23.79	0.653	0.360	4.17	46.07
Restoreformer++	25.09	0.657	0.352	4.12	39.98
DR2	23.55	0.595	0.434	4.20	50.13
DifFace	25.18	0.680	0.461	<u>4.01</u>	48.98
StableSR	24.99	0.671	0.361	4.60	50.50
PASD	<u>25.19</u>	0.698	0.419	7.77	67.05
TD-BFR(Ours)	25.21	<u>0.683</u>	0.347	3.99	<u>43.92</u>

Table III

QUANTITATIVE COMPARISONS OF FID ON LFW-TEST, WIDER-TEST, AND CELEBCHILD-TEST. **BOLD** AND UNDERLINED INDICATE THE BEST AND THE SECOND BEST PERFORMANCE.

Methods	LFW-Test		WIDER-Test		CelebChild-Test	
	NIQE \downarrow	FID \downarrow	NIQE \downarrow	FID \downarrow	NIQE \downarrow	FID \downarrow
CodeFormer	4.34	53.62	4.28	60.72	4.82	113.42
GFP-GAN	4.36	53.19	4.32	65.18	4.65	114.19
GPEN	5.28	51.98	5.38	71.85	5.57	122.18
VQFR	3.95	52.50	4.10	59.87	4.50	112.90
Restoreformer++	<u>3.93</u>	49.60	<u>3.93</u>	<u>58.27</u>	4.42	105.98
DR2	4.08	50.86	4.32	67.44	<u>4.27</u>	121.53
DifFace	3.98	48.08	4.22	59.29	4.58	112.37
StableSR	4.48	48.59	4.38	58.32	4.80	115.90
PASD	5.52	46.35	10.78	139.96	5.21	135.53
TD-BFR(Ours)	3.91	<u>47.88</u>	3.88	57.59	4.19	<u>110.55</u>

metric (NIQE), with SSIM and FID ranking second. Fig. 4 shows qualitative comparisons with SOTA methods. Non-diffusion methods often introduce artifacts, particularly around the mouth, while diffusion methods like DR2 and DifFace exhibit significant artifacts, and StableSR and PASD are overly smooth. In contrast, our method, utilizing diffusion priors and a truncated structure, generates high-quality facial images with minimal artifacts, preserving identity.

Real-world Datasets. Tab. III shows quantitative comparisons of NIQE and FID on real-world datasets, where TD-BFR achieves the best NIQE and ranks second in FID. Fig. 5 presents three examples, excluding underperforming

non-diffusion methods (GFPGAN and Restoreformer++) for brevity (full results in the supplementary material). Previous BFR methods often produce hazy or unnatural faces, especially under severe degradations (Row 3). In contrast, our method generates natural, detailed results, preserving features like wrinkles and eyes.

D. Ablation studies

Baseline. Since Stage 3, GDB serves as the detail generation module, it retains some restoration capabilities even without LRS and ADR. Therefore, we conducted ablation experiments using GDB as the baseline.

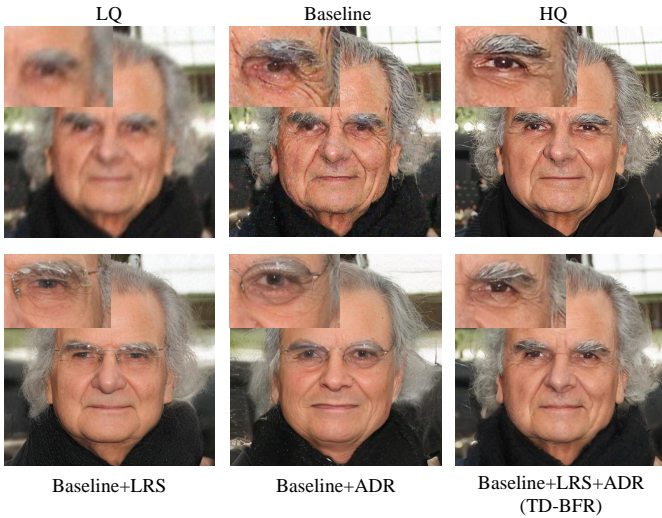


Figure 6. Visual comparison of ablation studies. (Zoom in for the best view)

Table IV
ABLATION STUDIES ON CELEBA-TEST DATASET. **BOLD** INDICATES THE BEST PERFORMANCE.

Methods	PSNR \uparrow	SSIM \uparrow	LPIPS \downarrow	FID \downarrow	Time(s)
Baseline	24.21	0.642	0.435	53.43	5.27
Baseline+LRS	24.52	0.657	0.433	53.01	4.68
Baseline+ADR	25.19	0.680	0.351	44.12	7.07
Baseline+LRS+ADR	25.21	0.683	0.347	43.92	3.53

Baseline + LRS. LRS improves sampling efficiency but has weaker degradation removal capabilities, leading to GDB generating results lacking fine details (see Fig. 6). The quantitative results are also significantly lower in Tab. IV.

Baseline + ADR. ADR, as the core degradation removal module, can produce comparable image quality when combined with the baseline (see Fig. 6). However, the absence of LRS results in more truncation steps at higher resolution, significantly reducing efficiency (see Tab. IV).

IV. CONCLUSION

We propose TD-BFR, a progressive framework for the BFR task, which significantly improves sampling speed by using incomplete diffusion models during inference. An ADR addresses unknown degradations and resolution variations, ensuring high-quality restoration through LRS and high-resolution GDB. Extensive experiments show that TD-BFR achieves comparable image quality to state-of-the-art methods while improving speed by **4.75 \times** on average.

V. ACKNOWLEDGMENTS

This work is supported by National Natural Science Foundation of China (62271308), STCSM (24ZR1432000, 24511106902, 24511106900, 22511105700, 22DZ2229005), 111 plan (BP0719010), and State Key Laboratory of UHD Video and Audio Production and Presentation.

REFERENCES

[1] Shangchen Zhou, Kelvin C.K. Chan, Chongyi Li, and Chen Change Loy, "Towards robust blind face restoration with codebook lookup transformer," in *NeurIPS*, 2022.

[2] Xintao Wang, Yu Li, Honglun Zhang, and Ying Shan, "Towards real-world blind face restoration with generative facial prior," in *Proceedings of the IEEE/CVF Conference on Computer Vision and Pattern Recognition*, 2021, pp. 9168–9178.

[3] Jonathan Ho, Ajay Jain, and Pieter Abbeel, "Denoising diffusion probabilistic models," *Advances in Neural Information Processing Systems*, vol. 33, pp. 6840–6851, 2020.

[4] Zhixin Wang, Ziyang Zhang, Xiaoyun Zhang, Huangjie Zheng, Mingyuan Zhou, Ya Zhang, and Yanfeng Wang, "Dr2: Diffusion-based robust degradation remover for blind face restoration," in *Proceedings of the IEEE/CVF Conference on Computer Vision and Pattern Recognition*, 2023, pp. 1704–1713.

[5] Jianyi Wang, Zongsheng Yue, Shangchen Zhou, Kelvin C.K. Chan, and Chen Change Loy, "Exploiting diffusion prior for real-world image super-resolution," in *arXiv preprint arXiv:2305.07015*, 2023.

[6] Zongsheng Yue and Chen Change Loy, "Difface: Blind face restoration with diffused error contraction," *IEEE Transactions on Pattern Analysis and Machine Intelligence*, 2024.

[7] Huangjie Zheng, Pengcheng He, Weizhu Chen, and Mingyuan Zhou, "Truncated diffusion probabilistic models," *arXiv preprint arXiv:2202.09671*, vol. 1, no. 3.1, pp. 2, 2022.

[8] Jiayan Teng, Wendi Zheng, Ming Ding, Wenyi Hong, Jianqiao Wang, Zhuoyi Yang, and Jie Tang, "Relay diffusion: Unifying diffusion process across resolutions for image synthesis," *arXiv preprint arXiv:2309.03350*, 2023.

[9] Yu Wang, Gencheng Wang, Rong Chen, and Yuzhen Chen, "An efficient diffusion for blind face restoration," in *Proceedings of the 2024 7th International Conference on Image and Graphics Processing*, 2024, pp. 340–347.

[10] Robin Rombach, Andreas Blattmann, Dominik Lorenz, Patrick Esser, and Björn Ommer, "High-resolution image synthesis with latent diffusion models," in *Proceedings of the IEEE/CVF conference on computer vision and pattern recognition*, 2022, pp. 10684–10695.

[11] Jooyoung Choi, Sungwon Kim, Yonghyun Jeong, Youngjune Gwon, and Sungroh Yoon, "Ilvr: Conditioning method for denoising diffusion probabilistic models," in *2021 IEEE/CVF International Conference on Computer Vision (ICCV)*. IEEE, 2021, pp. 14347–14356.

[12] Tim Brooks, Aleksander Holynski, and Alexei A. Efros, "Instruct-pix2pix: Learning to follow image editing instructions," in *Proceedings of the IEEE/CVF Conference on Computer Vision and Pattern Recognition (CVPR)*, June 2023, pp. 18392–18402.

[13] Tao Yang, Peiran Ren, Xuansong Xie, and Lei Zhang, "Pixel-aware stable diffusion for realistic image super-resolution and personalized stylization," *arXiv preprint arXiv:2308.14469*, 2023.

[14] Tero Karras, Samuli Laine, and Timo Aila, "A style-based generator architecture for generative adversarial networks," in *Proceedings of the IEEE/CVF conference on computer vision and pattern recognition*, 2019, pp. 4401–4410.

[15] Ziwei Liu, Ping Luo, Xiaogang Wang, and Xiaoou Tang, "Deep learning face attributes in the wild," in *Proceedings of the IEEE international conference on computer vision*, 2015, pp. 3730–3738.

[16] Shuo Yang, Ping Luo, Chen-Change Loy, and Xiaoou Tang, "Wider face: A face detection benchmark," in *Proceedings of the IEEE conference on computer vision and pattern recognition*, 2016, pp. 5525–5533.

[17] Gary B Huang, Marwan Mattar, Tamara Berg, and Eric Learned-Miller, "Labeled faces in the wild: A database for studying face recognition in unconstrained environments," in *Workshop on faces in 'Real-Life' Images: detection, alignment, and recognition*, 2008.

[18] Chaofeng Chen, Dihong Gong, Hao Wang, Zhifeng Li, and Kwan-Yee K Wong, "Learning spatial attention for face super-resolution," *IEEE Transactions on Image Processing*, vol. 30, pp. 1219–1231, 2020.

[19] Tao Yang, Peiran Ren, Xuansong Xie, and Lei Zhang, "Gan prior embedded network for blind face restoration in the wild," in *Proceedings of the IEEE/CVF Conference on Computer Vision and Pattern Recognition*, 2021, pp. 672–681.

[20] Zhouxia Wang, Jiawei Zhang, Tianshui Chen, Wenping Wang, and Ping Luo, "Restoreformer++: Towards real-world blind face restoration from undegraded key-value pairs," *IEEE Transactions on Pattern Analysis and Machine Intelligence*, 2023.

[21] Yuchao Gu, Xintao Wang, Liangbin Xie, Chao Dong, Gen Li, Ying Shan, and Ming-Ming Cheng, "Vqfr: Blind face restoration with vector-quantized dictionary and parallel decoder," in *ECCV*, 2022.